Engineering Structures, 221 (2020), ARTN 111093
https://doi.org/10.1016/j.engstruct.2020.111093

Cyclic Deformation Characteristics of S355 and S690 Steels under Different Loading Protocols

[a,b] **Guo Y.B.**, [a,b] **Ho H.C.,** [a,b] **Chung K.F.* and** [c] **Elghazouli A.Y.**

[a] Department of Civil and Environmental Engineering
The Hong Kong Polytechnic University, Hong Kong SAR, China.

[b] Chinese National Engineering Research Centre for Steel Construction (Hong Kong Branch)
The Hong Kong Polytechnic University, Hong Kong SAR, China.

[c] Department of Civil and Environmental Engineering, Imperial College London, U.K.

**Corresponding author: kwok-fai.chung@polyu.edu.hk*

Abstract

Despite of excellent high strength to self-weight ratios of the S690 steels, when compared with the S355 steels, there is a widespread concern regarding the ductility of the S690 steels. It is generally considered that the ductility of the S690 steels is significantly lower than that of the S355 steels – this is the general understandings the authors attempt to investigate.

This paper presents an experimental investigation into cyclic deformation characteristics of both S355 and S690 steels through low-cycle high-strain cyclic tests with two different loading protocols. A detailed account of the results of 32 cyclic tests on both the S355 and the S690 funnel-shaped coupons is presented. Effects of four different target strains and two different loading frequencies are also examined in details. For the ranges of loading protocols, strain amplitudes, and frequencies considered, the hysteretic responses of these coupons of the two steels are compared directly in terms of engineering stress-strain curves based on their nominal diameters. Microstructures of the fractured coupons of the two steels are also identified for comparison.

Contrary to the general understandings, it is demonstrated that the high strength S690 steels do have a good ductility under both monotonic and cyclic actions. Moreover, depending on specific loading protocols and target strains, the cyclic deformation characteristics of the S690 steels are demonstrated to be superior to those of the S355 steels in terms of the number of cycles completed prior to failure and their corresponding energy dissipation characteristic under various target strains up to ±10.0%.

The findings of this experimental investigation highlight the importance of establishing ductility requirements and cyclic deformation characteristics for the high strength S690 steels in accordance with specifically designed cyclic tests rather than relying solely on conventional monotonic tensile tests.

Keywords

High strength steel; cyclic deformation characteristics; hysteretic behaviour; loading protocols; cyclic ductility requirements.

1 Introduction

High strength steels commonly refer to materials with a nominal yield strength larger than 460 N/mm^2. In recent years, high strength S690, S890 and S960 steels have become readily available in many countries. These high strength steels are widely considered as efficient construction materials owing to their high strength-to-weight ratios. In the past two decades, high strength steels have been used in a number of applications, particularly for heavily loaded structural members of large machines and lifting equipment. Compared to normal strength S355 steels, a wider application of high strength steels in construction will reduce member sizes and self-weights of structural members, hence leading to a significant reduction in construction cost and time. It is thus highly attractive for structural engineers to employ high strength steels in structures such as high-rise buildings and long span bridges.

Typically, the S355 steels are considered to possess a relatively high level of ductility which allows structural members in various commonly adopted structural forms to undergo large deformations at full plastic section resistances. However, there is a widespread concern regarding the ductility of the higher strength steels, which is generally considered to be significantly lower compared to the normal strength S355 steels. Due to the lack of relevant design recommendations, it is unclear whether direct adoption of the high strength S690 steels in such structures would deliver similar behaviour in comparison with the S355 steels. Consequently, there is a need to quantify the ductility properties of the high strength S690 steels, with respect to that of S355 steels.

There are simple, yet important, clauses on ductility requirements for structural steels in various codes and standards. For those commonly used S235 to S460 steels, the ductility requirements stipulated in EN 1993-1-1 [1] are given as follows:

i)	f_u / f_y	$\geq$	1.10;	1a)
ii)	ε_L	$\geq$	15 %; and	1b)
iii)	ε_u	$\geq$	15 ε_y	1c)

where f_y and f_u are the yield and the tensile strengths of the steel; ε_L is the strain at failure; ε_u is the strain corresponding to f_u ; and ε_y is the strain corresponding to f_y.

For the high strength S690 steels under consideration in this paper, relevant ductility requirements are given in EN 1993-1-12 [2] instead, and they are given as follows:

iv)	f_u / f_y	$\geq$	1.05;	2a)
v)	ε_L	$\geq$	10 %; and	2b)
vi)	ε_u	$\geq$	15 ε_y	2c)

It should be noted that these requirements are primarily based on test results obtained from monotonic tensile tests. It is generally recognized that the high strength S690 steels behave differently from those S235 and S460 steels, owing to their different forms of microstructures produced to different manufacturing methods and delivery conditions [3-7]. Moreover, the mechanical properties of these steels obtained from the monotonic tensile tests are often found to be very different [8, 9] to those obtained from cyclic tests. Therefore, there is a need to investigate simultaneously the structural responses of both the S355 and the S690 steels directly from monotonic tensile tests as well as cyclic tests in order to establish whether the concern on reduced ductility in the high strength S690 steels is justified. More importantly, a ductility requirement based on cyclic actions would be highly relevant in deciding whether the high strength S690 steels should be adopted in seismic resistant structures.

1.1 Common loading protocols for cyclic tests

In order to assess mechanical properties of the high strength S690 steels under cyclic actions, it is essential to adopt suitable loading protocols with specific ranges of strain amplitudes which vary in a format with relevant magnitudes and frequencies [8, 9, 23, 24]. According to the existing testing standards, there are many loading protocols for cyclic tests proposed by various researchers for a wide range of engineering disciplines [10-15]. For those loading protocols closely relevant to the present investigation into the cyclic deformation characteristics of the S690 steels, they may be classified into two main categories:

i) Cyclic testing with constant strain amplitudes

As shown in Figure 1a), this protocol [10-12] is widely accepted as a standard protocol to assess cyclic deformation characteristic of the steel coupons under specific ranges of target strains and loading frequencies. Their performance in these tests is assessed through the number of the cycles completed under specific target strains before fracture, and the corresponding energy dissipated during testing. This protocol is very effective in identifying any cyclic deterioration in strength in the steel coupons during testing.

ii) Cyclic testing with varying strain amplitudes

As shown in Figure 1b), a pre-determined pattern of strain variations to FEMA 461 [13-15] with increasing amplitudes is imposed to the steel coupons. The performance of the steel coupons is assessed as whether a pre-determined target strain can be attained after a total of 20 cycles. In general, this protocol is widely considered to be highly appropriate for structural assessments of constructional materials and structural members against seismic actions.

A number of researchers [16-25] have reported their investigations into the cyclic deformation characteristics of different types of steels using various testing methods and loading protocols for specific structural applications. In general, some researchers assessed fatigue behaviour of high strength steels [16-20], including fracture mechanisms and microstructure changes at elevated temperatures. Others focused on evaluating various mechanical behaviour of high strength steels under different target strains over a wide range of strain rates [21-24]. However, these investigations are conducted to a wide range of non-standard loading protocols which do not necessarily relate to any specific application.

In general, no systematic experimental investigation into cyclic responses of the high strength steels and their members under practical ranges of seismic actions is reported, and hence, it is difficult to assess whether the high strength steels should be adopted in seismic resistant structures. This is, indeed, an uncharted area in existing design standards and codes of practice. Hence, there is an urgent need to conduct systematic comparative studies to generate new understandings, and to formulate a rational ductility requirement for qualifying the high strength steels to be used to build seismic resistant structures.

1.2 Previous research by the authors

As a pilot study into the hysteretic behavior of the high strength S690 steels, a systematic experimental investigation was conducted by the authors [8] in which a total of 36 monotonic and cyclic tests on specially designed coupons, namely, funnel-shaped coupons, of the S690 steels were conducted. Both the geometry and the dimensions of these coupons are illustrated in Figure 2. All of these coupons were tested under a loading protocol with varying amplitudes and different loading frequencies according to FEMA 461 [14]. It should be noted that under

the loading protocol, both the target strains ε_m and the loading frequencies f were selected according to typical ranges of seismic actions encountered in infrastructure. To be more specific, the values of the target strains ε_m were set to range from ±2.5 to ±10.0% with an interval of ±2.5%, and these cyclic actions were applied at four different loading frequencies f, i.e. 0.1, 0.5, 1.0 and 2.0 Hz, in these cyclic tests.

The main conclusions from these tests are summarized as follows:

- In the cyclic tests, a total of 28 out of the 36 coupons were able to complete all the 20 cycles under the loading protocol of varying strain amplitudes with target strains ε_m up to ±7.5% and the loading frequencies f up to 2.0 Hz.
- However, a total of 8 coupons fractured pre-maturely at the 20th cycle when the target strain ε_m at ±10.0% was adopted, and the same failure was recorded at all the four different loading frequencies.
- Varying loading frequencies over the range of 0.1 to 2.0 Hz was found to have little effects on the hysteretic behavior of these S690 steels.
- Owing to large deformations taken place in the coupons during the cyclic tests, there was a significant increase (or reduction) in the cross-sectional areas of the coupons under varying compressive (or tensile) applied forces. Hence, it is important to evaluate true stresses in these coupons based on the instantaneous diameters of these coupons.

Hence, these tests provide an opportunity to examine structural responses of the high strength S690 steels under those cyclic actions which are directly relevant to seismic loadings in structures. Experience gained in conducting these tests as well as in interpreting test results are also helpful in selecting suitable loading protocols, target strains and loading frequencies in conducting subsequent cyclic tests of the high strength steels. It will be highly desirable to further examine the cyclic deformation characteristics of the S690 steels under different loading protocols with more stringent demands as well as to carry out comparative studies with the S355 steels to quantify differences in their cyclic responses.

1.3 Objective and scope of work

This paper describes a detailed experimental investigation into the cyclic deformation characteristics of both the S355 and the S690 steels in order to determine whether concerns related to perceived reduced ductility in the S690 steels are justified. More importantly, a ductility requirement based on cyclic behaviour will be of direct relevance to applicability of the S690 steels for dissipative seismic performance. It should be noted that the research work reported in this paper is part of a research programme which is devised to examine both mechanical properties of the S690 steels and structural behaviour of their welded sections and joints under i) monotonic actions, and ii) cyclic actions. The research programme aims to facilitate structural engineers to use the high strength S690 steels in heavily loaded members in high-rise buildings and long span bridges.

In the present study, the following specific tasks are conducted:

- Task A Monotonic tensile tests

  A total of 4 monotonic tensile tests on standard funnel-shaped coupons of both the S355 and the S690 steels are undertaken to obtain basic mechanical test data for comparison.

- Task B Cyclic tension / compression tests

  A total of 16 S355 funnel-shaped coupons, and 16 S690 funnel-shaped coupons are conducted under two different loading protocols, namely:

  i) Loading Protocol C with constant strain amplitudes, as shown in Figure 1a), and

ii) Loading Protocol V with varying strain amplitudes, as shown in Figure 1b).

- Task C Microstructural identification

  Images of microstructures of both the S355 and the S690 tested coupons are obtained using a high power optical microscope, and differences in the microstructures of both the S355 and the S690 steels in the fractured regions are identified. Through systematic digital imaging analyses, volumetric fractions of both the S355 and the S690 steels are also quantified.

Key areas of interest of the present investigation include:

a) the number of cycles completed prior to failure, n_c , under different loading protocols for both the S355 and the S690 steels with 4 different target strains ε_m , and 2 different loading frequencies f ;

b) cyclic deformation characteristics of both the S355 and the S690 steels in terms of engineering stress-strain (σ_e - ε_e) curves; and

c) a direct comparison of hysteretic behaviour and energy dissipation characteristic of both the S355 and the S690 steels under different loading protocols.

As shown in Table 1, typical chemical compositions of both the S355 and the S690 steels adopted in the present study are shown to be in full compliance with the requirements given in EN 10025-2 and 10025-6. For example, both Phosphorus (P) and Sulphur (S) are limited to a maximum content of 0.025% and 0.012% respectively. It should be noted that both Phosphorus (P) and Sulphur (S) will have detrimental effects onto the mechanical properties [25] of the steels.

Figure 2 illustrates the dimensions of the standard funnel-shaped coupons employed in the present study according to a number of testing methods [10-12] on cyclic tests. These coupons are specially devised for cyclic tests, and they are considered to be suitable up to strains of 10 ~ 15% although buckling of the central portions of the coupons may occur at large axial shortenings, depending on the strength and the dimensions of the coupons as well as the test set-up. All the monotonic and the cyclic tests were conducted with a Universal Fatigue Testing Machine Instron 8803 with a capacity of 500 kN, as illustrated in Figure 3.

2 Monotonic Tensile Tests

In order to obtain the basic material properties of both the S355 and the S690 steels considered, a total of 4 monotonic tensile tests on funnel-shaped coupons were carried out in accordance with BS EN ISO 6892-1 [26], and the test programme is shown in Table 2. A high precision Instron Dynamic Extensometer 2620-603 with a gauge length of 10.000 mm was used to measure the elongations of the coupons with an accuracy of 0.0015 mm. Figure 4 shows typical fractured coupons of both the S355 and the S690 steels after the monotonic tensile tests. It is shown that tensile fracture takes place in the central core of the coupons while shear fracture is evident in the circumferential edges of the coupons.

Figure 5a) depicts the engineering stress-strain (σ_e - ε_e) curves for both the S355 and the S690 steels, which are plotted onto the same graph for direct comparison. It is shown that both the S355 and the S690 steels exhibit a linear deformation under initial loading application up to their yield points, followed by a nonlinear deformation with different extents of hardening. The following points are worth noting:

- The S355 steels exhibit significant strain hardening from the initial yielding up to a deformation of 8%. After that, the amount of strain hardening is less pronounced, and

significant softening occurs after an initiation of necking in the coupons at a strain of about 10%.

- The S690 steels exhibit distinctly different deformation characteristics, when compared with those of the S355 steels. After yielding, only a limited amount of strain hardening occurs up to a strain of about 3.5%. Softening is then evident thereafter up to the occurrence of fracture.

The mechanical properties of both the S355 and the S690 steels are summarized in Table 2. As the maximum value of the coefficients of variation is 4%, dispersion in their mechanical properties is considered to be relatively small.

3 Cyclic Axial Tests

In order to investigate the cyclic deformation characteristics of both the S355 and the S690 steels, a total of 16 S355 funnel-shaped coupons and 16 S690 funnel-shaped coupons were tested under the following two different loading protocols:

a) Loading Protocol C
In each cyclic test, a pre-determined strain amplitude, i.e. a target strain ε_m , was adopted in which the cyclic action was applied to the coupon through a carefully monitored deformation control so that the maximum strain in the coupon varied alternately from $+\varepsilon_m$ (a tensile strain) to $-\varepsilon_m$ (a compressive strain). It should be noted that the target strain was kept to be a constant throughout the test, and the test was only terminated after fracture of the coupon. The number of cycle completed prior to fracture, n_c , was registered at the end of the test.

b) Loading Protocol V
A loading protocol with varying strain amplitudes as specified in FEMA-461 was adopted in which the cyclic action was applied to the coupon through a carefully monitored deformation control so that the strain amplitude in the coupon varied alternately from a tensile strain to a compressive strain. It should be noted that as the value of the strain amplitude was increased by a factor of 1.4 at every other cycle as specified for moderate seismicity, the initial value of the strain amplitude was selected in such a way that after a total of 9 increments, the final value of the strain amplitude was equal to the target strain, ε_m . It should be noted that the test was terminated after successful completion of the 20^{th} cycle or fracture of the coupon. The number of cycle completed prior to fracture, n_c , was registered at the end of the test.

For both loading protocols, a total of four target strains are adopted, i.e. $\varepsilon_m = \pm 2.5\%, \pm 5.0\%, \pm 7.5\%$ and $\pm 10.0\%$ while the loading frequencies f are specified at 0.1 and 1.0 Hz. Table 3 summarizes the programme of the cyclic tests for both the S355 and the S690 steels. It should be noted that all the cyclic tests are conducted using the Universal Fatigue Testing Machine Instron 880, and the high precision Instron Dynamic Extensometer 2620-603 is employed to measure deformations as well as to monitor strains of the coupons throughout the tests.

All the tests have been conducted successfully, and Table 4 gives the numbers of cycles completed prior to fracture, n_c , in all the cyclic tests conducted in the present investigation. Typical fractured coupons after cyclic testing are shown in Figure 6, noting that the ripples that appear on the fractured surfaces are very different from those observed in the monotonic tests.

3.1 Engineering stress-strain (σ_e - ε_e) curves under Loading Protocol C with f = 0.1 Hz

All the measured engineering stress-strain (σ_e - ε_e) curves of the cyclic tests are plotted in various graphs in Figure 7 for direct comparison. It should be noted that:

a) For those cyclic tests under Loading Protocol C with ε_m at ±2.5% and ±5.0%:

- It is evident that these engineering stress-strain (σ_e - ε_e) curves of the S355 steels may be considered as effective hysteretic loops, indicating good energy dissipation under these ranges of cyclic actions. Moreover, these loops exhibit insignificant softening after repeated cyclic actions.

- The engineering stress-strain (σ_e - ε_e) curves of the S690 steels are also considered as effective hysteretic loops, but there is a more pronounced cyclic deterioration in their strengths, especially after a large number of cycles have been completed.

- The S355 and the S690 steels are able to complete 85 and 58 cycles, respectively, when the target strain ε_m is ±2.5%. When the target strain ε_m is increased to ±5.0%, the corresponding values of n_c are found to be decreased to 13 and 16 respectively.

b) For those cyclic tests under Loading Protocol C with ε_m at ±7.5% and ±10.0%:

- The engineering stress-strain (σ_e - ε_e) curves of the S355 steels may be considered as effective hysteretic loops, indicating good energy dissipation under these ranges of cyclic actions.

- The engineering stress-strain (σ_e - ε_e) curves of the S690 steels are also considered as effective hysteretic loops, but there is a more notable deterioration in their strengths, especially after a large number of cycles have been completed.

- The numbers of cycles completed prior to fracture, n_c , for the S355 and the S690 steels under cyclic actions with a target strain ε_m at ±7.5% are found to be 5 and 8 respectively. When the target strain ε_m is increased to ±10.0%, the corresponding values of n_c are found to be decreased to 4 and 6 respectively. Hence, it is demonstrated that the S690 steels are able to attain more cycles completed prior to fracture, compared to the S355 steels, when the target strains ε_m are at ±7.5% and ±10.0%.

3.2 Engineering stress-strain (σ_e - ε_e) curves under Loading Protocol V with f = 0.1 Hz

All the measured engineering stress-strain (σ_e - ε_e) curves of the cyclic tests are plotted together in various graphs in Figure 8 for direct comparison. It should be noted that:

a) For the cyclic tests under Loading Protocol V with ε_m at ±2.5% and ±5.0%:

- It is evident that the engineering stress-strain (σ_e - ε_e) curves of the S355 steels overlap one another almost completely when plotted together, and hence, their cyclic deformations are both stable and robust under repeated cyclic actions.

- However, the engineering stress-strain (σ_e - ε_e) curves of the S690 steels are different as there are inconsistent deformation characteristics after repeated cyclic actions, especially in the initial ranges of the cyclic actions.

- Both the S355 and the S690 steels are able to complete 20 cycles prior to fracture when the target strains are equal to either ±2.5% or ±5.0%, i.e. the numbers of cycles completed prior to fracture, n_c , are found to be 20 in all these cases.

b) For the cyclic tests under Loading Protocol V with ε_m at ±7.5% and ±10.0%

- The engineering stress-strain (σ_e - ε_e) curves of the S355 steels are shown to be stable and robust while those of the S690 steels are shown to have more pronounced strength deterioration under repeated cyclic actions.

- The values of n_c for both the S355 and the S690 steels are found to be 20 when the target strain ε_m is ±7.5%. However, when the target strain ε_m is increased to ±10.0%, the values of n_c for both the S355 and the S690 steels are reduced to 19. Importantly, it should be noted that the S690 steels are able to attain the same number of cycles prior to fracture as the S355 steels.

3.3 Engineering stress-strain (σ_e - ε_e) curves under Loading Protocols C and V with f = 1.0 Hz

All the measured engineering stress-strain (σ_e - ε_e) curves of these cyclic tests are plotted together in Figures 9 and 10 for direct comparison. It should be noted that:

a) For cyclic tests carried out under Loading Protocol C:

- As shown in Figure 9, the engineering stress-strain (σ_e - ε_e) curves of the S355 steels are shown to be stable and robust while those of the S690 steels are shown to have more pronounced strength deterioration under repeated cyclic actions.

- The values of n_c for both the S355 and the S690 steels are found to be reduced steadily when the target strain ε_m increases. Table 4 provides a detailed comparison of these values.

b) For cyclic tests carried out under Loading Protocol V:

- As shown in Figure 10, the engineering stress-strain (σ_e - ε_e) curves of the S355 steels are shown to be stable and robust while those of the S690 steels exhibit more significant softening under repeated cyclic actions.

- The values of n_c for both the S355 and the S690 steels are found to be reduced steadily when the target strain ε_m increases. Table 4 provides a detailed comparison of these values.

It is important to note that, in general, the cyclic deformation characteristics of the S355 and the S690 steels under the two Loading Protocols and various target strains are found to be insignificantly affected by loading frequency, i.e. whether f is 0.1 or 1.0 Hz. In other words, the effect of loading frequency is shown to be considerably less pronounced than commonly anticipated.

Overall, it is shown that these cyclic tests are able to identify different cyclic deformation characteristics of the S355 and the S690 steels. These differences are evident in terms of the engineering stress-strain (σ_e - ε_e) curves, as well as in the number of cycles completed prior to fracture, and also with respect to any strength deterioration after repeated cyclic actions.

3.4 Microstructures of S355 and S690 steels

In order to identify microstructural differences between the S355 and the S690 steels, a metallurgical investigation was carried out. Fractured coupons after the cyclic tests as reported above were cut into halves along their longitudinal directions, as shown in Figures 11 and 12, using a temperature controlled EDM wire cutting. They were then ground using silicon carbide papers of grades 60, 120, 240, 320, 400, 600 and 800 sequentially, and then, polished using 1 μm diamond paste on an automatic rotating disc at approximately 250 r.p.m. Finally, they were etched using a 2~5 % Nital solution to distinguish their microstructural texture.

Images of the microstructures were obtained with the use of a high power optical microscope Leica DM LM at two different locations of a typical fractured coupon, as shown in Figures 11b) and 12b) for the S355 and the S690 steels respectively. It should be noted that these images of the fractured region at Point P and the un-necked region at Point Q were captured with a magnification of 920 times. It is shown that:

a) Owing to different chemical compositions, heat treatment and delivery conditions, these steels possess different microstructures which exhibit different mechanical properties in terms of strengths and deformations under loadings [25]. Moreover, there are significant microstructural distortions near the fractured regions of the coupons, as shown in both Figures 11c) and 12c), as a result of repeated tension and compression deformations during testing.

b) After systematic digital imaging analyses, the volumetric fractions of various phases of the steels are determined as follows:

   - The fractured coupon of the S355 steels is identified as a microstructure of retained austenite with a volumetric fraction of pearlite in a ferrite matrix of 24.7%.
   - However, the fractured coupon of the S690 steels is shown to be a microstructure of about 99% tempered martensite together with various retained phases.

Hence, these images provide important microstructural evidence on the mechanical behaviour of the high strength steels after large cyclic deformations.

4 Hysteretic Behaviour of S355 and S690 Steels

In order to quantify the comparative hysteretic behaviour of both the S355 and the S690 steels under different loading protocols, the normalized engineering stress ratio β_e is employed, and it is defined as follows:

$$\beta_e = \sigma_e / f_y \qquad 3)$$

Based on the above, the following curves are established:

a) Normalized engineering stress ratio versus engineering strain (β_e - ε_e) curves for cyclic tests under Loading Protocol C.

   Figure 13 illustrates the normalized engineering stress ratio versus engineering strain (β_e - ε_e) curves for both the S355 and the S690 steels under cyclic actions of constant strain

amplitudes. It is shown that both steels exhibit satisfactory hysteretic responses, attaining different numbers of cycles completed prior to fracture, n_c , at various target strains ε_m .

Importantly, the number of cycles completed prior to fracture, n_c , at various target strains for the S690 steels are larger than those values of the S355 steels, when the target strains ε_m are ±5.0%, ±7.5% and ±10.0%.

b) Normalized engineering stress ratio versus engineering strain (β_e - ε_e) curves for cyclic tests under Loading Protocol V

Figure 14 illustrates the normalized engineering stress ratio versus engineering strain (β_e - ε_e) curves for both the S355 and the S690 steels under cyclic actions of varying strain amplitudes. The dashed lines also depict the backbone curves of these curves. It is shown that both steels provide satisfactory hysteretic responses, and all of them are able to attain 20 cycles, i.e. n_c = 20 when the target strains ε_m are ±2.5%, ±5.0%, and ±7.5%. When the target strains ε_m are ±10.0%, both steels can only attain 19 completed cycles, i.e. n_c = 19. Hence, the hysteretic behaviour of both the S355 and the S690 steels under cyclic actions with varying strain amplitudes is shown to be very similar.

Consequently, both Loading Protocols C and V are considered to be necessary in quantifying the hysteretic behaviour of both the S355 and the S690 steels under cyclic actions. The number of cycles completed prior to fracture n_c under specific Loading Protocols with various target strains ε_m are considered to be key parameters for both the S355 and the S690 steels in quantifying their hysteretic responses under low-cycle high-strain cyclic actions, as summarized in Table 4. It should be noted that both the S355 and the S690 steels are shown to have comparable cyclic ductility under both Loading Protocols C and V.

4.1 Comparative energy dissipation performances of both S355 and S690 steels

It is important to assess energy dissipation characteristic of the S355 and the S690 steels according to the engineering stress-strain (σ_e - ε_e) curves derived in Section 3. By summing up the areas enclosed by each set of the curves [27, 28] in the graphs in Figures 7 to 10, various kinds of energy dissipated per unit volume of steel in these cyclic tests under Loading Protocol C are obtained. It should be noted that the use of engineering stresses and engineering strains to determine energy dissipation is commonly accepted in structural level, but not in materials level.

Figure 15 plots the energy dissipated per unit volume of steel in each cycle of the tests for both the S355 and the S690 steels under different target strains and loading frequencies. The energy dissipated per unit volume of steel in each cycle of the S690 steels are consistently higher than those of the S355 steels, in particular, when the target strain ε_m = ±5.0, ±7.5 and ±10%.

Table 5 summarizes the total energy dissipated per unit volume of steel, E , of both the S355 and the S690 steels under different target strains and loading frequencies. It is shown that under Loading Protocol C:

a) The total energy dissipated per unit volume of steel of the S690 steels, E_1 , is about 0.81 to 0.84 of those of the S355 steels, E_0 , when the target strain ε_m is ±2.5%.

b) However, when the target strains ε_m are increased to ±5.0, ±7.5 and ±10.0%, the corresponding total energy dissipated per unit volume of steel of the S690 steels, E_1 , are significantly larger than those of the S355 steels , E_0 , by a factor ranging from 1.56 to 2.07.

c) After dividing the total energy dissipated per unit volume of steel, E , by the number of cycles completed before fracture, n_c , the average energy dissipated per unit volume of steel per cycle, e , are obtained. It is important to note that the values of e_1 of the S690 steels are significantly larger than those of the S355 steels, e_0 , and their ratios are shown to vary narrowly between 1.23 and 1.33 for all cases covered in the study.

The total energy dissipated per unit volume of steel, E , are plotted in Figure 22a) while the corresponding average values per cycle, e , are shown in Figure 22b). In general, it is shown that the energy dissipation characteristic of the S690 steels is superior to that of the S355 steels when the target strains ε_m are ±5.0, ±7.5 and ±10% under both loading frequencies. Moreover, the effect of the loading frequency, f , onto the energy dissipation characteristics is shown to be less pronounced than commonly anticipated.

5 Conclusions

Despite of excellent high strength to self-weight ratios of the S690 steels, when compared with the S355 steels, there is a widespread concern regarding the ductility of the S690 steels. It is generally considered that the ductility of the S690 steels is significantly lower than that of the S355 steels – this is the general understandings the authors attempt to investigate.

A systematic experimental investigation into the cyclic deformation characteristics of both the S355 and the S690 steels under different loading protocols is presented in this paper. A total of 4 monotonic tensile tests on funnel-shaped coupons were firstly conducted in order to obtain the basic mechanical properties of both the S355 and the S690 steels. These were followed by cyclic tests on 16 S355 and 16 S690 funnel-shaped coupons, which were tested under: i) Loading Protocol C with constant strain amplitudes, and ii) Loading Protocol V with varying strain amplitudes, both with four target strains ε_m , namely, ±2.5, ±5.0, ±7.5 and ±10%, and two loading frequencies f, namely, 0.1 and 1.0 Hz.

Key findings from the experimental investigation are summarized as follows:

a) Deformation characteristics of the S355 and the S690 steels have been examined under monotonic tensile tests. They are found to be very different when expressed in terms of engineering stress-strain (σ_e - ε_e) curves, and they exhibit different levels of strain hardening immediately after yielding as well as in the post yielding ranges.

b) Cyclic deformation characteristics of the S355 and the S690 steels have been examined under the two Loading Protocols. In general, the stress-strain curves of both the S355 and the S690 steels are found to exhibit various degrees of softening under repeated cyclic actions. The number of cycles completed prior to fracture under the two Loading Protocols with different target strains and loading frequencies are summarized in Table 4 for direct comparison. Moreover, the energy dissipation characteristics of both the S355 and the S690 steels are presented in Table 5 according to the two Loading Protocols with various target strains and loading frequencies.

c) It is important to compare cyclic deformation characteristics of the S355 and the S690 steels under specific loading protocols as well as specific target strains and loading frequencies. Based on the test results summarized in Tables 4 and 5, it is found that:

i. Contrary to the general understandings on the ductility of both the S355 and the S690 steels, the cyclic deformation characteristics of both steels are demonstrated to be the same under Loading Protocol V with all the four target strains and the two loading frequencies !

ii. The cyclic deformation characteristics of the S690 steels are demonstrated to be inferior to that of the S355 steels under Loading Protocol C with a target strain ε_m at ±2.5% and f = 0.1 and 1.0 Hz. This agrees with the general understandings.

iii. Interestingly, the cyclic deformation characteristics of the S690 steels are demonstrated to be superior to that of the S355 steels under Loading Protocol C with target strains ε_m at ±5.0, ±7.5 and ±10%, and f = 0.1 and 1.0 Hz. This is contrary once again to the general understandings !

Consequently, the experimental evidence allows the international research community for structural engineering and modern steel construction technology to appreciate that the high strength S690 steels do have a good ductility under both monotonic and cyclic actions. Moreover, depending on specific loading protocols and target strains, the cyclic deformation characteristics of the S690 steels are demonstrated to be superior to those of the S355 steels. The findings of this experimental investigation highlight the importance of establishing ductility requirements and cyclic deformation characteristics for the high strength S690 steels in accordance with specifically designed cyclic tests rather than relying solely on conventional monotonic tensile tests. The experimental investigation will be further extended to examine cyclic deformation characteristics of welded sections of the S355 and the S690 steels, and this will be reported in due course.

Acknowledgements

The research work reported in this paper is part of a project under a comprehensive research programme entitled "Sustainable Infrastructure Development with Modern Steel Construction Technology" of the Chinese National Engineering Research Centre for Steel Construction (Hong Kong Branch) of the Hong Kong Polytechnic University. The CNERC is funded by the Innovation and Technology Fund of the Innovation and Technology Commission of the Government of the Hong Kong SAR, and the Research Committee of the Hong Kong Polytechnic University (Project Nos. 1-BBY3, BBY6 & BBV3). The research work is also partially funded by the Research Grants Council of the University Grants Committee of the Government of Hong Kong SAR (Project Nos.: 152687/16E, 152231/17E and 157152/18E). Financial support (Project No. RJKB) for the research study of the first author from the Research Committee of the Hong Kong Polytechnic University is gratefully acknowledged. Special thanks are also sincerely expressed to the technicians of the Structural Engineering Unit of the Department of Civil and Environmental Engineering of the Hong Kong Polytechnic University.

References

[1] BS EN 1993-1-1. Design of Steel Structures – Part 1–1: General rules and rules for buildings. British Standards Institution; 2005.

[2] BS EN 1993-1-12. Design of Steel Structures – Part 1–12: Additional rules for the extension of EN 1993 up to steel grades S700. British Standards Institution; 2007.

[3] BS EN 10025-1: 2004. Hot rolled products of structural steels – Part 1: General technical delivery conditions. British Standards Institution.

[4] BS EN 10025-2: 2004. Hot rolled products of structural steels – Part 1: Technical delivery conditions for non-alloy structural steels. British Standards Institution.

[5] BS EN 10025-3: 2004. Hot rolled products of structural steels – Part 1: Technical delivery conditions for normalized/normalized rolled weldable fine grain structural steels. British Standards Institution.

[6] BS EN 10025-4: 2004. Hot rolled products of structural steels – Part 1: Technical delivery conditions for thermomechanical rolled weldable fine grain structural steels. British Standards Institution.

[7] BS EN 10025-6: 2004. Hot rolled products of structural steels – Part 1: Technical delivery conditions for flate products of high strength structural steels in the quenched and tempered condition. British Standards Institution.

[8] Ho HC, Liu X, Chung KF, Elghazouli AY, and Xiao M. (2018). Hysteretic behaviour of high strength S690 steel materials under low cycle high strain tests. Engineering Structures 165: 222-236.

[9] Wang YB, Li GQ, Sun X, Chen SW, and Hai LT. (2017). Evaluation and prediction of cyclic response of Q690D steel. Proceedings of the Institution of Civil Engineers - Structures and Buildings, 170.11: 788-803.

[10] ISO 12106. Metallic materials –fatigue testing – Axial-strain-controlled method. Switzerland: International Organization for Standardization; 2003.

[11] ASTM E606/E606M-12. Standard Test Method for Strain-Controlled Fatigue Testing. ASTM International, 100 Barr Harbor Drive, PO Box C700, West Conshohockem, PA.

[12] GB/T 15248. Metallic materials – constant amplitude strain controlled axial fatigue – method of test. Beijing, China: Standard Press of China; 1994 [In Chinese].

[13] ECCS. Seismic design. Recommended testing procedure for assessing the behaviour of structural steel elements under cyclic loads. Technical Committee 1 – Structural safety and loadings. TWG 1.3 Rep. No. 45, 1986.

[14] FEMA-461. (2007). Interim testing protocols for determining the seismic performance characteristics of structural and non-structural components. Washington, D.C., U.S.A: Federal Emergency Management Agency, Department of Homeland Security.

[15] ANSI-AISC 341-16. Seismic Provisions for Structural Steel Buildings, Standard, American Institute of Steel Construction, Chicago, Illinois, USA, 2016.

[16] Chen Y, Sun W, and Chan TM. Effect of loading protocols on the hysteresis behaviour of hot-rolled structural steel with yield strength up to 420 MPa. Advanced Structural Engineering, 2013, 16(4): 707–19.

[17] Fournier B, Sauzay M, Caës C, Noblecourt M, and Mottot M. Analysis of the hysteresis loops of a martensitic steel – Part I: Study of the influence of strain amplitude and temperature under pure fatigue loadings using an enhanced stress partitioning method. Material Science and Engineering, A 2006, 437: 183–96.

[18] Fournier B, Sauzay M, Caës C, Mottot M, Noblecourt M, and Pineau A. Analysis of the hysteresis loops of a martensitic steel – Part II: Study of the influence of creep and stress relaxation holding times on cyclic behaviour. Materials Science and Engineering, A 2006, 437: 197–211.

[19] Khan S, Wilde F, Beckmann F, and Mosler J. Low cycle fatigue mechanism of the lightweight alloy Al2024. International Journal of Fatigue 2012, 38: 92–9.
[20] Li Y, Pan X, Wang and G. Low cycle fatigue and ratcheting properties of steel 40Cr under stress controlled tests. International Journal of Fatigue 2013, 55: 74–80.
[21] Nip KH, Gardner L, Davies CM, and Elghazouli AY. Extremely low cycle fatigue tests on structural carbon steel and stainless steel. Journal of Constructional Steel Research, 2010, 66: 96–110.
[22] Zhou F, Chen Y, and Wu Q. Dependence of the cyclic response of structural steel on loading history under large inelastic strains. Journal of Constructional Steel Research, 2015, 104: 64–73.
[23] Hu F and Shi G. Constitutive model for full-range cyclic behavior of high strength steel without yield plateau. Construction and Building Materials, 162(2018):596-607.
[24] Wang YB, Li GQ, Cui W, Chen SW, and Sun FF. Experimental investigation and modeling of cyclic behavior of high strength steel. Journal of Constructional Steel Research, 2015, 104: 37–48.
[25] Dieter GE. Mechanical metallurgy. New York, U.S.A.: McGraw-Hill; 1961.
[26] BS EN ISO 6892-1. (2009). Metallic materials – Tensile testing: Part 1: Method of test at ambient temperature, British Standards Institution.
[27] GOŁOŚ K. and Ellyin F. (1988). A total strain energy theory for cumulative fatigue damage. Transaction ASME, Journal of Pressure Vessel Technology, 110: 35-41.
[28] Ellyin F. (1989). A criterion for fatigue under multiaxial fatigue failure. Biaxial and Multiaxial Fatigue, EGF3, (Edited by K.J. Miller and M.W. Brown), Mechanical Engineering Publications, London, 571-583.

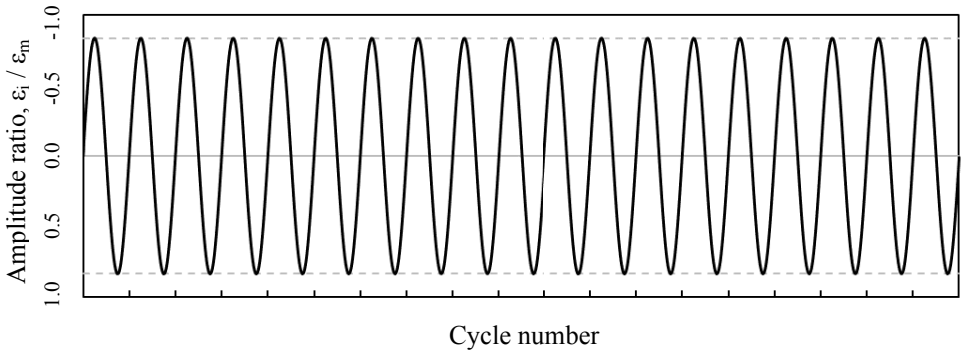

a) Loading Protocol C with constant strain amplitudes

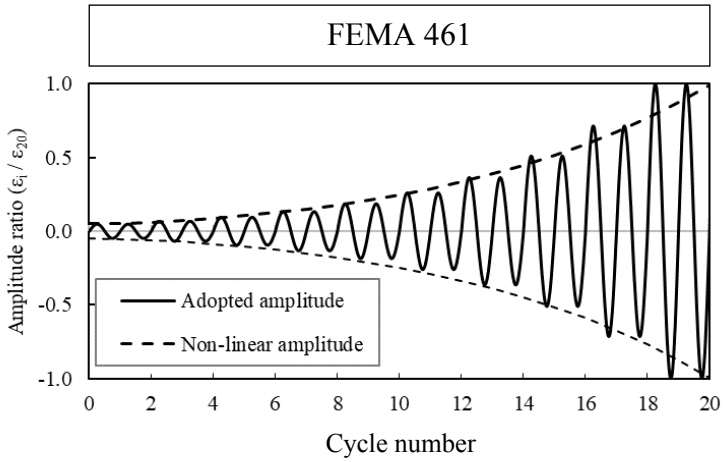

b) Loading Protocol V with varying strain amplitudes

Figure 1. Loading protocols of two different cyclic actions

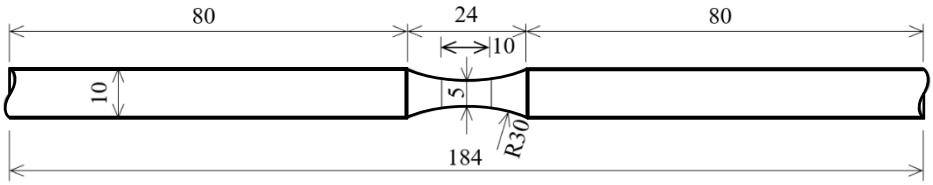

Figure 2. Geometry and dimensions of a typical funnel-shaped coupon

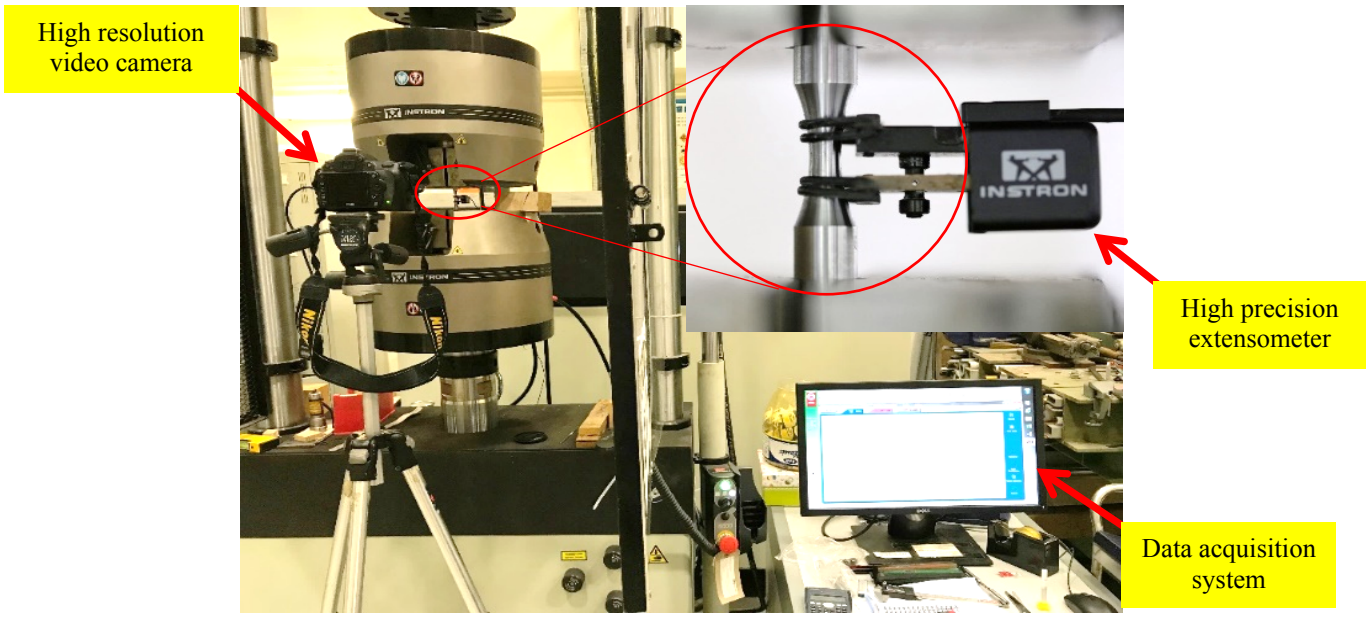

Figure 3. Test set-up for both monotonic and cyclic tests

a) Typical funnel-shaped coupon before testing

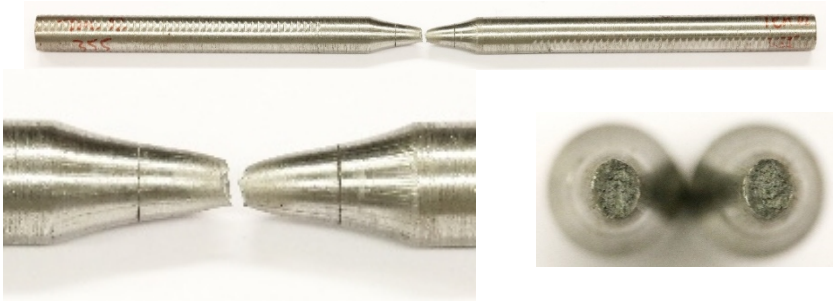

b) Fractured S355 coupon after test

c) Fractured S690 coupon after test

Figure 4 Funnel-shaped coupons under monotonic tensile tests

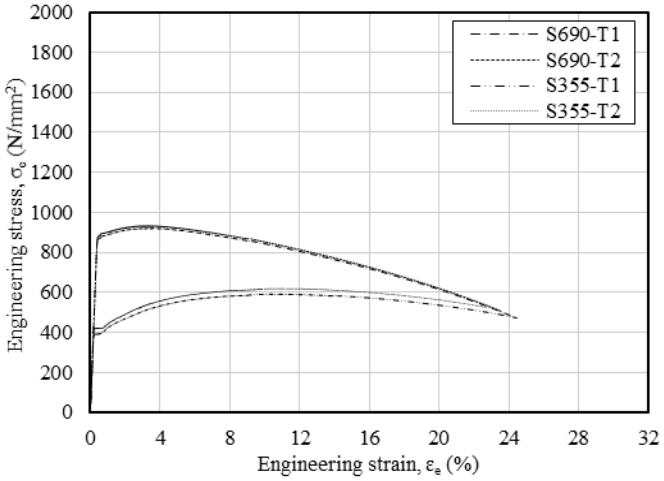

Figure 5 Measured engineering stress-strain $(\sigma_e - \varepsilon_e)$ curves of funnel-shaped coupons under monotonic tensile tests

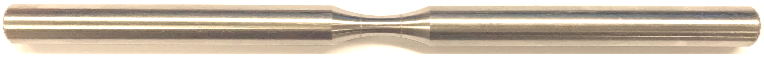

a) Typical funnel-shaped coupon before testing

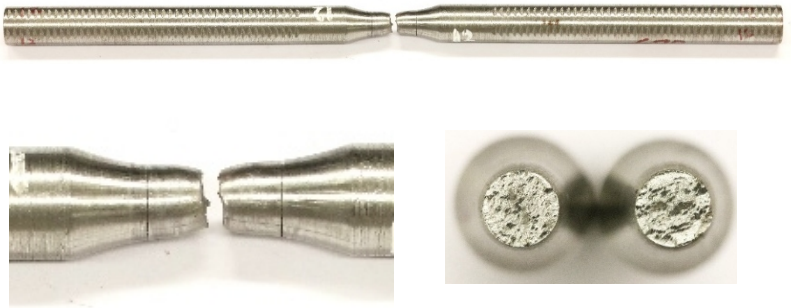

b) Fractured S355 coupon after test

c) Fractured S690 coupon after test

Figure 6 Funnel-shaped coupons under cyclic tests

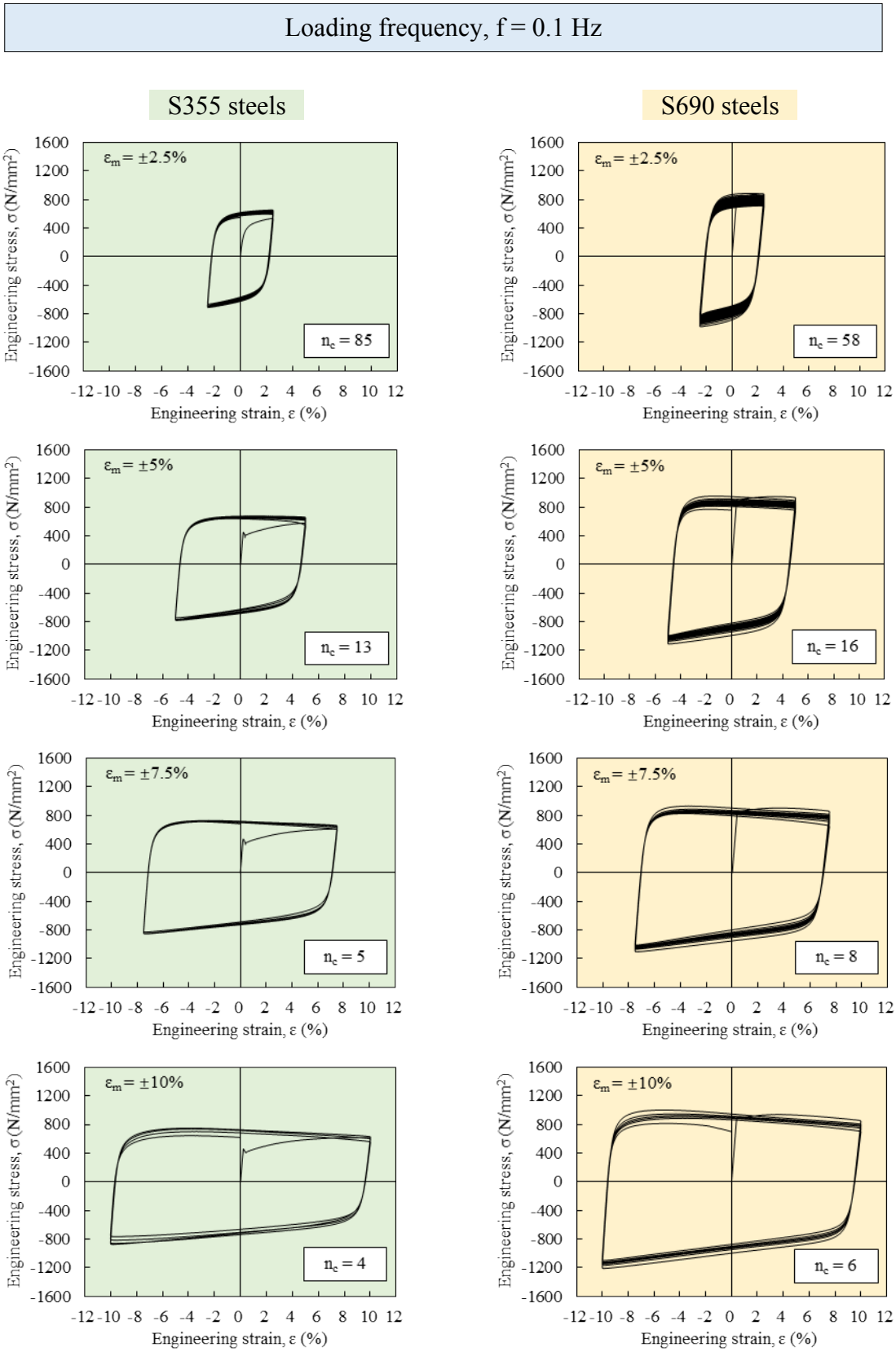

Figure 7 Engineering stress-strain (σ_e- ε_e) curves under Loading Protocol C with f = 0.1 Hz

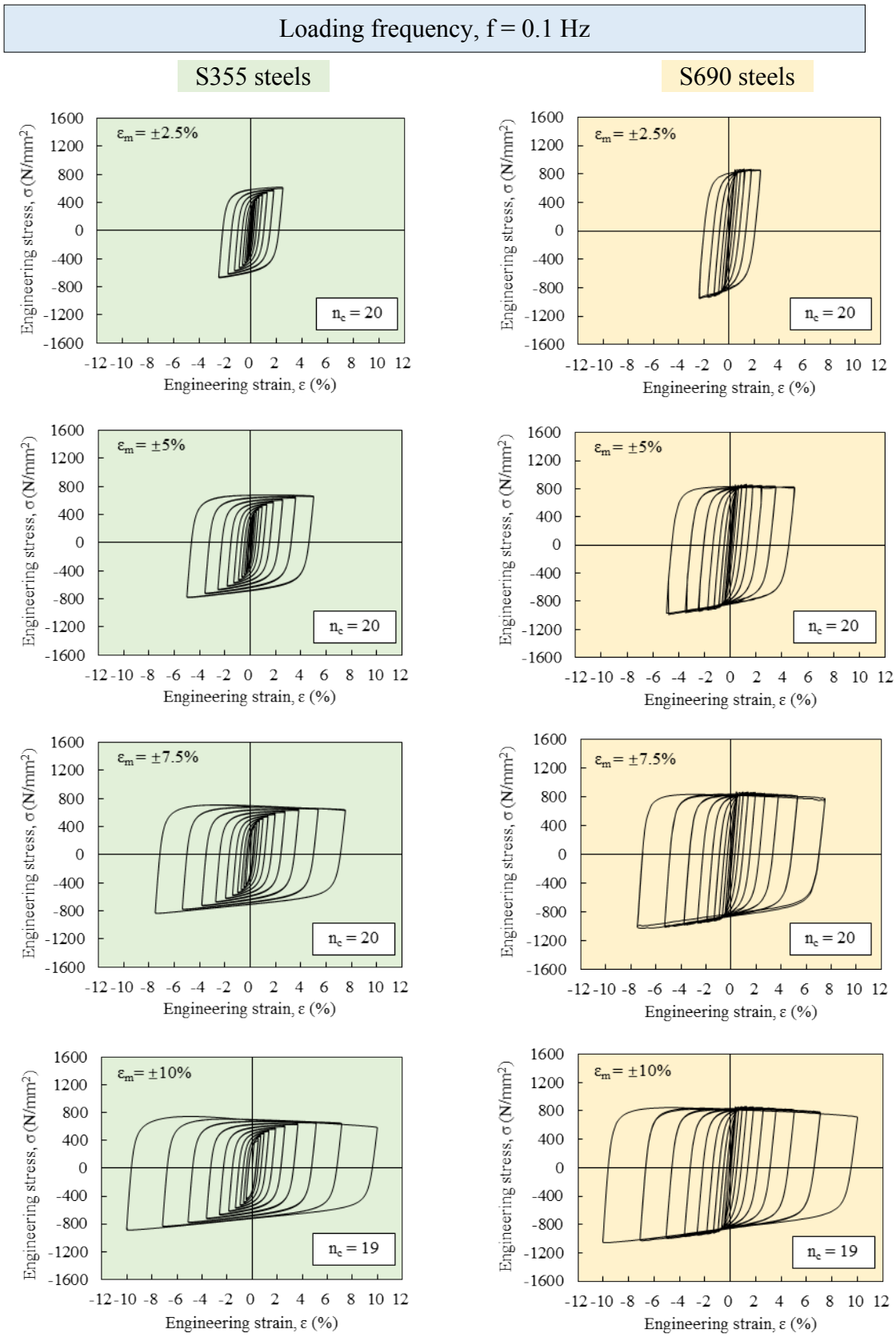

Figure 8 Engineering stress-strain (σ_e- ε_e) curves under Loading Protocol V with f = 0.1 Hz.

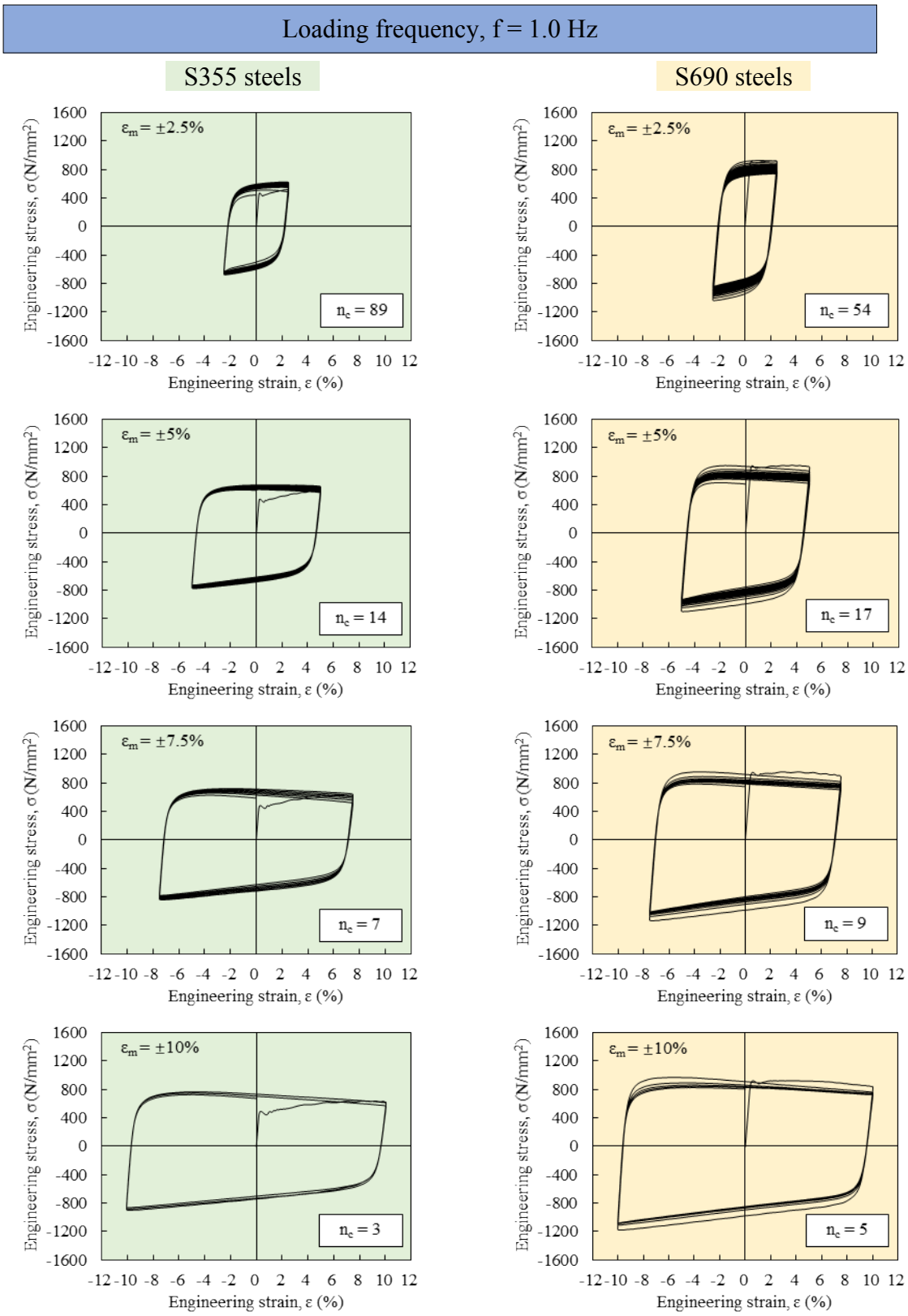

Figure 9 Engineering stress-strain (σ_e - ε_e) curves under Loading Protocol C with f = 1.0 Hz.

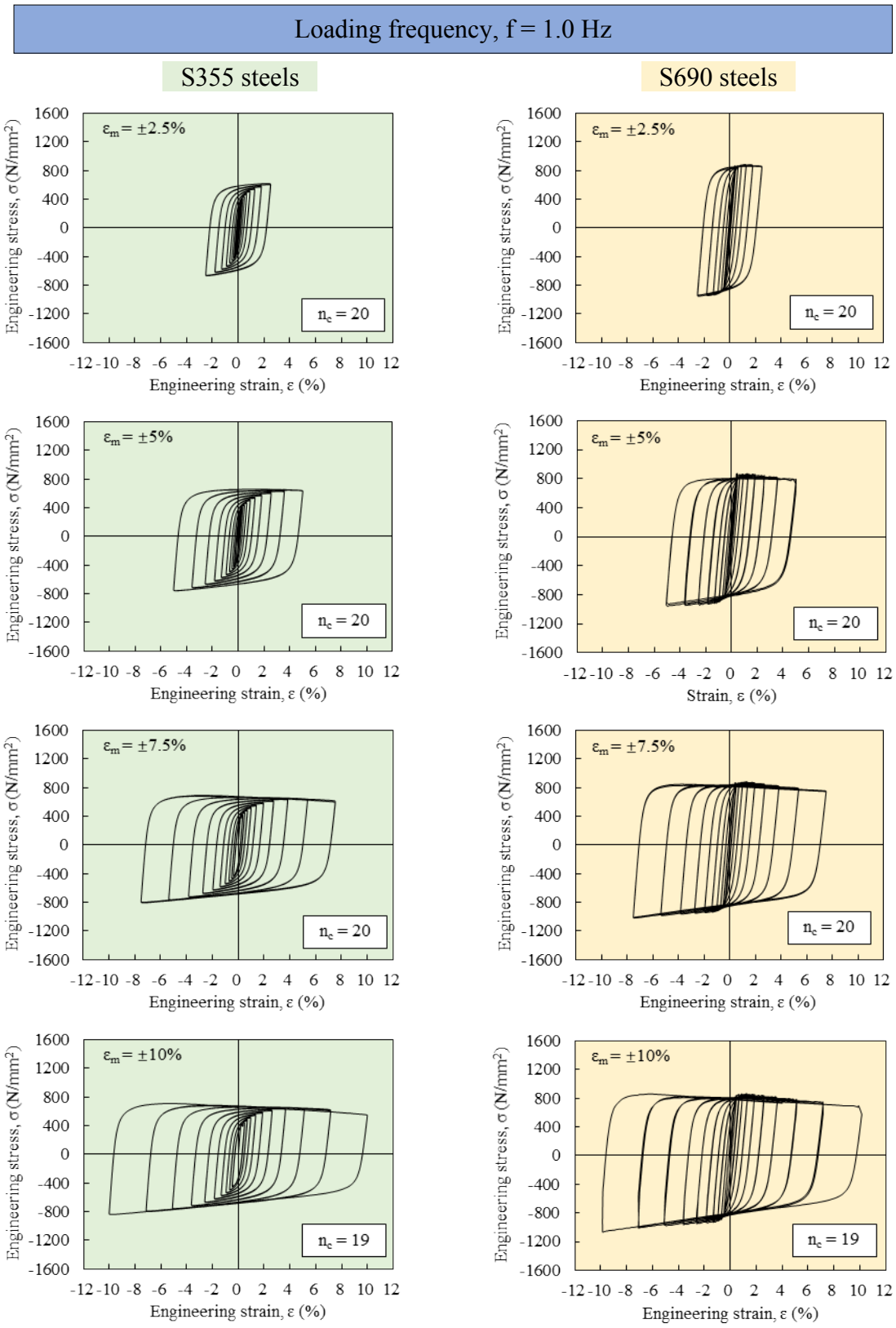

Figure 10 Engineering stress-strain (σ_e- ε_e) curves under Loading Protocol V with f = 1.0 Hz.

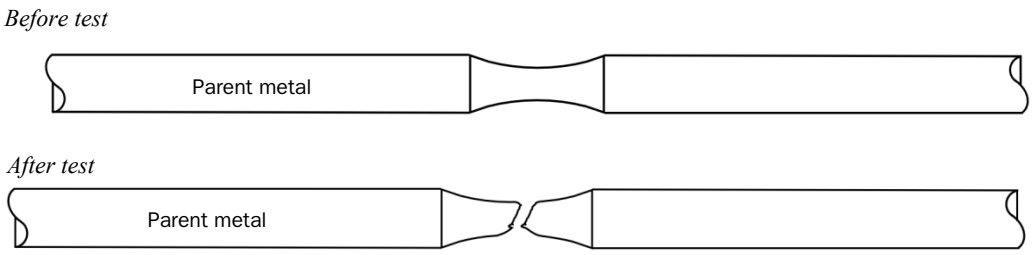

a) Macroscopic view of a test coupon of S355 steels

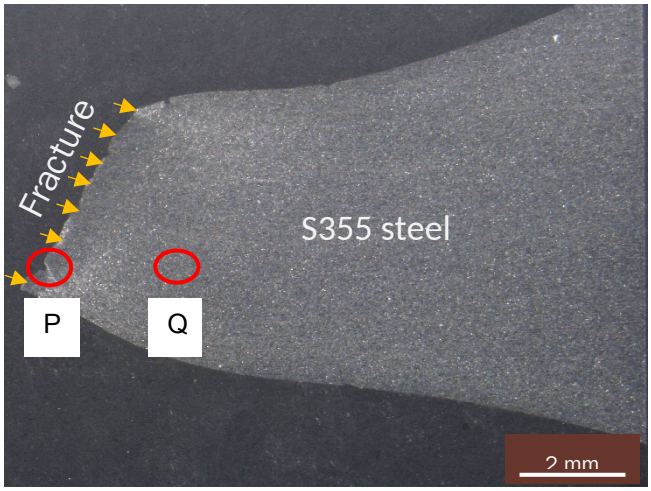

b) Longitudinal sectional view of the fractured coupon

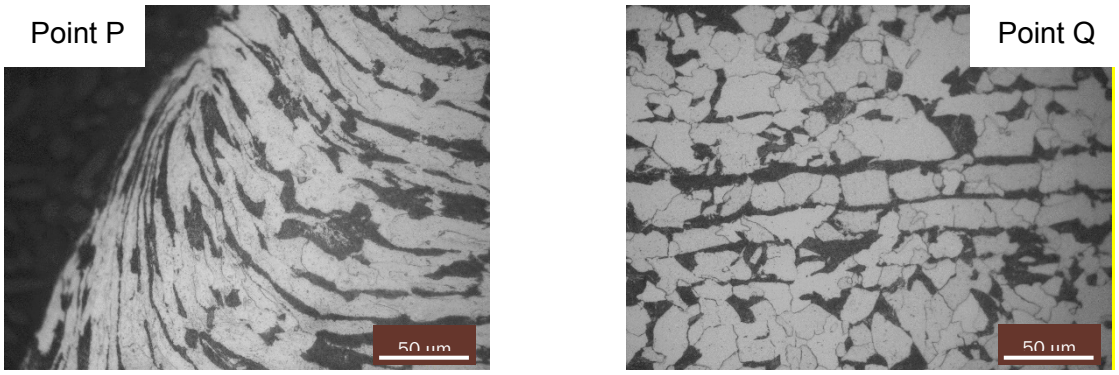

Microstructures (ferrite and pearlite) within the necking zone

Microstructures (ferrite and pearlite) outside the necking zone

c) OM images at Points P and Q (with a magnification at 920 times)

Figure 11. Macroscopic and microscopic views of typical fractured coupon of S355 steels - Loading Protocol C with $\varepsilon_m = \pm 10.0\%$ and f = 0.1 Hz

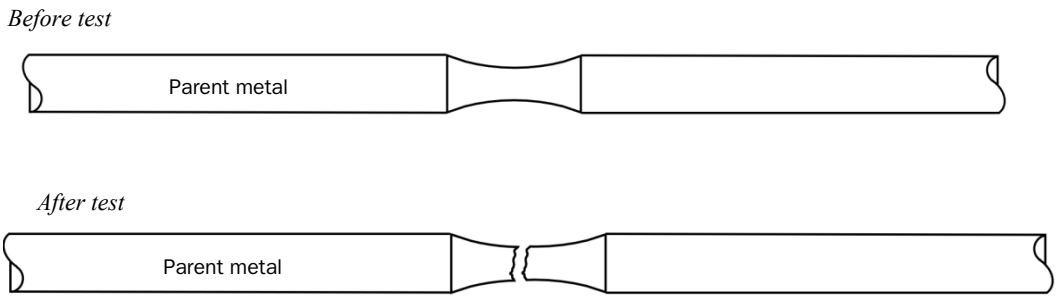

a) Macroscopic view of a test coupon of S690 steels

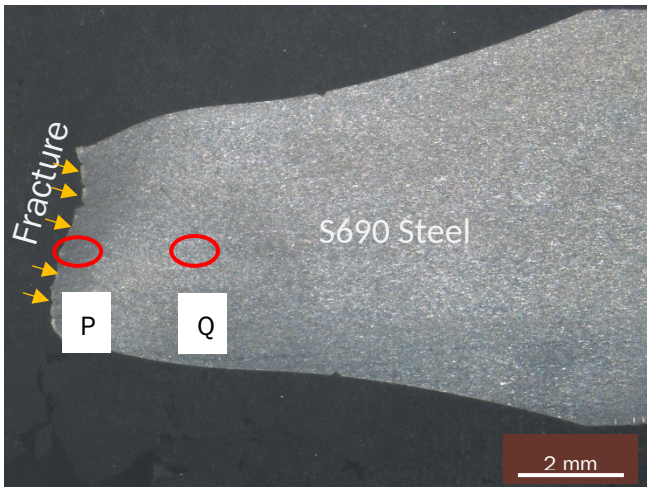

b) Longitudinal sectional view of the fractured coupon

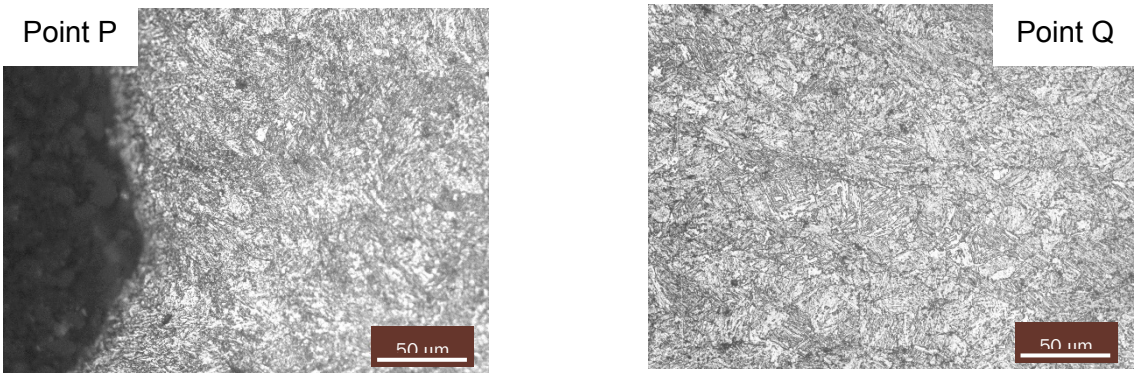

Microstructures (tempered martensite) within the necking zone

Microstructures (tempered martensite) outside the necking zone

c) OM images at Points P and Q (with a magnification at 920 times)

Figure 12. Macroscopic and microscopic views of typical fractured coupon of S690 steels - Loading Protocol C with $\varepsilon_m = \pm 10.0\%$ and f = 0.1 Hz

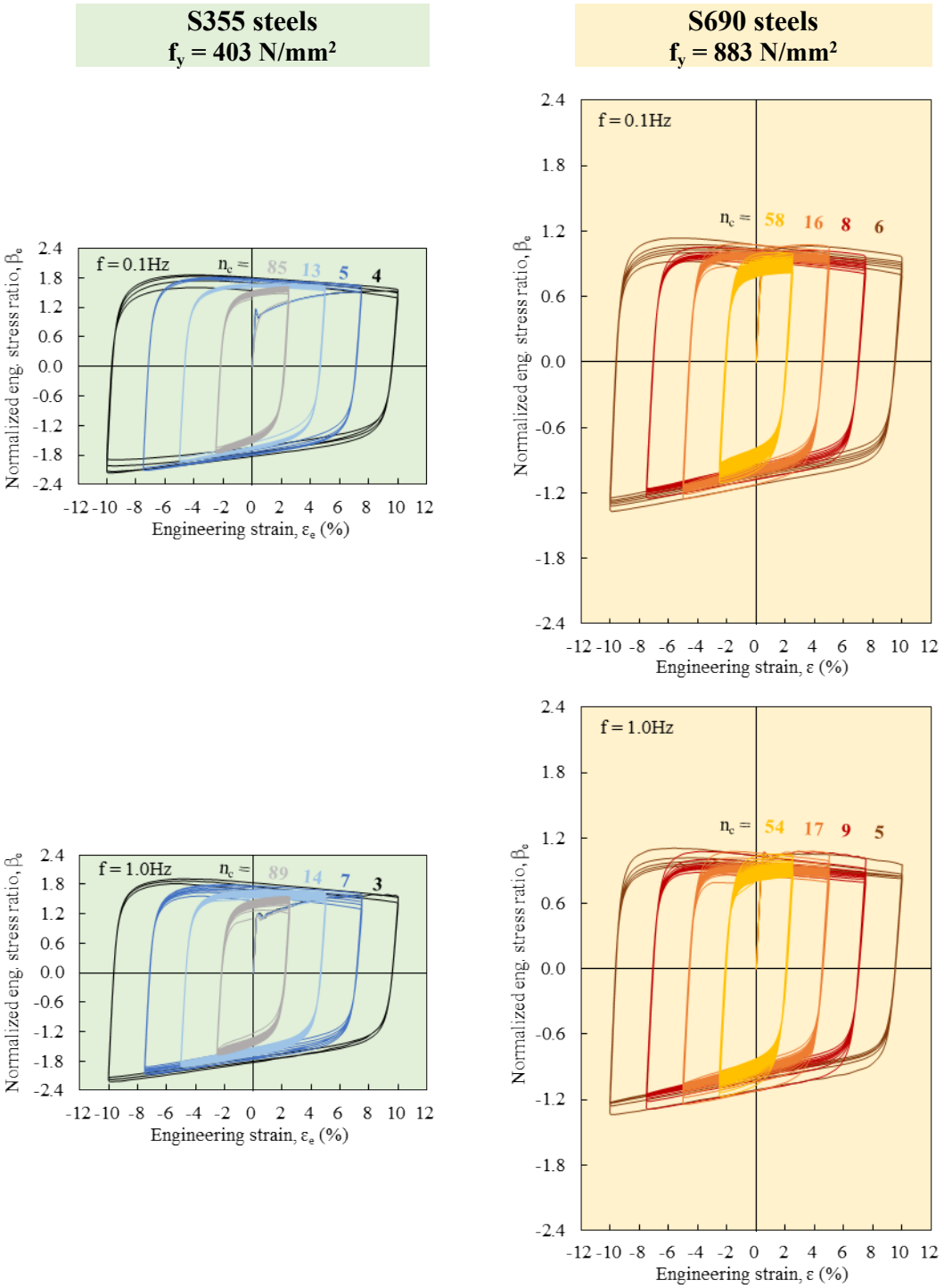

Figure 13 Hysteretic curves of both S355 and S690 steels under Loading Protocol C with various target strains and loading frequencies.

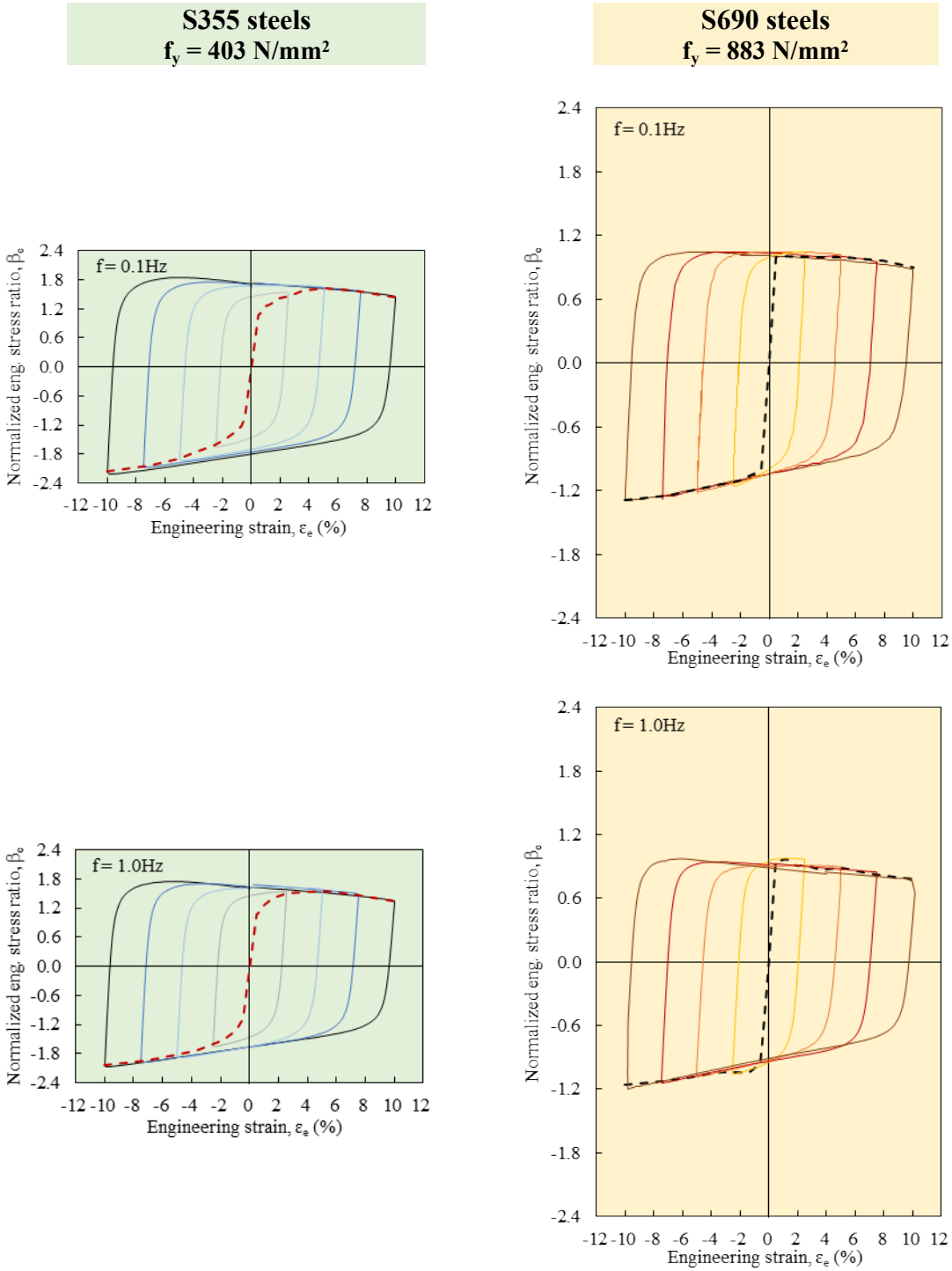

Figure 14 Hysteretic curves of both S355 and S690 steels under Loading Protocol V with various target strains and loading frequencies.

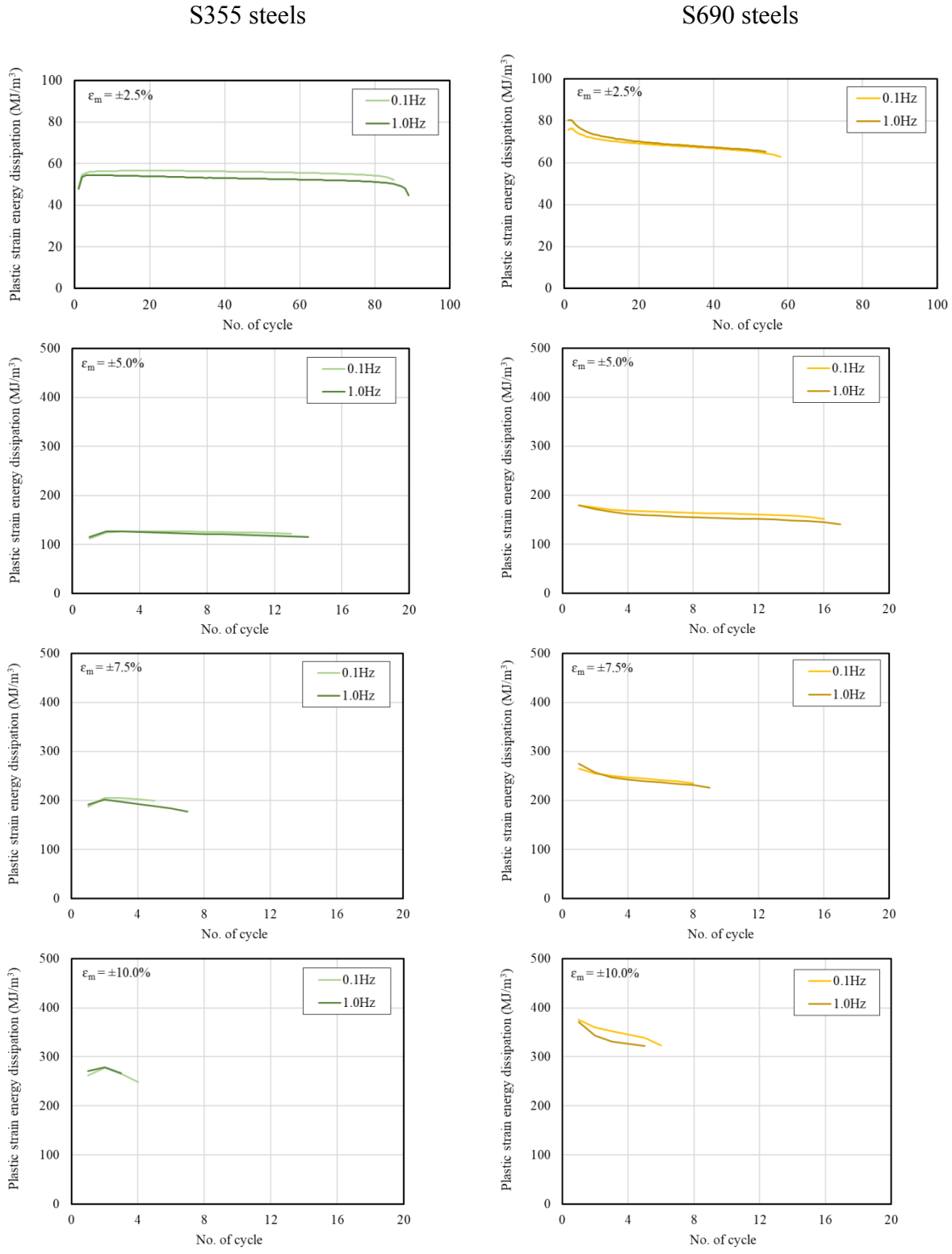

Figure 15 Energy dissipation characteristics against number of cycles of both S355 and S690 steels under Loading Protocol C

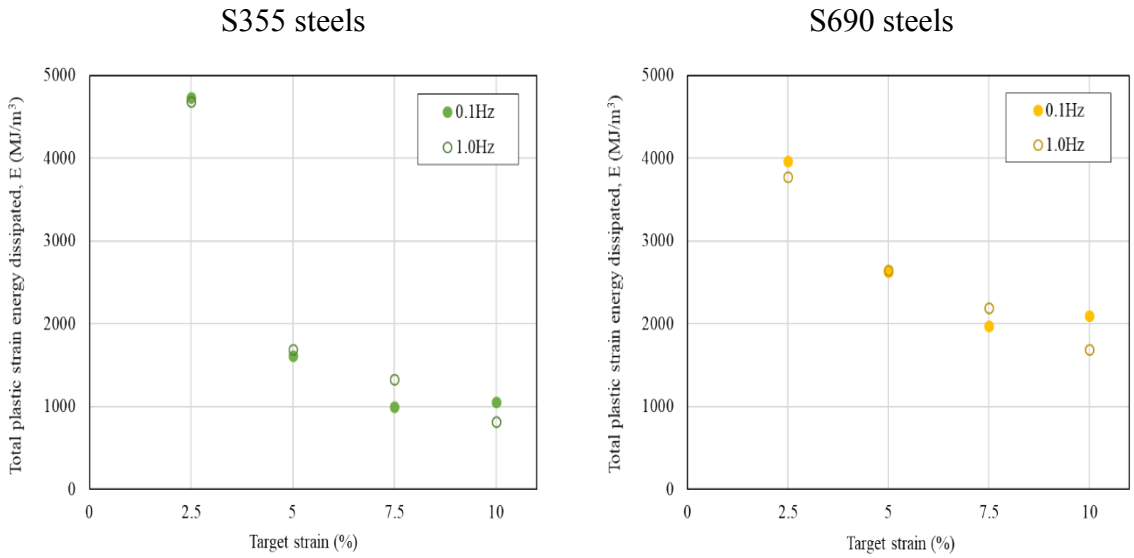

a) Total energy dissipated per unit volume

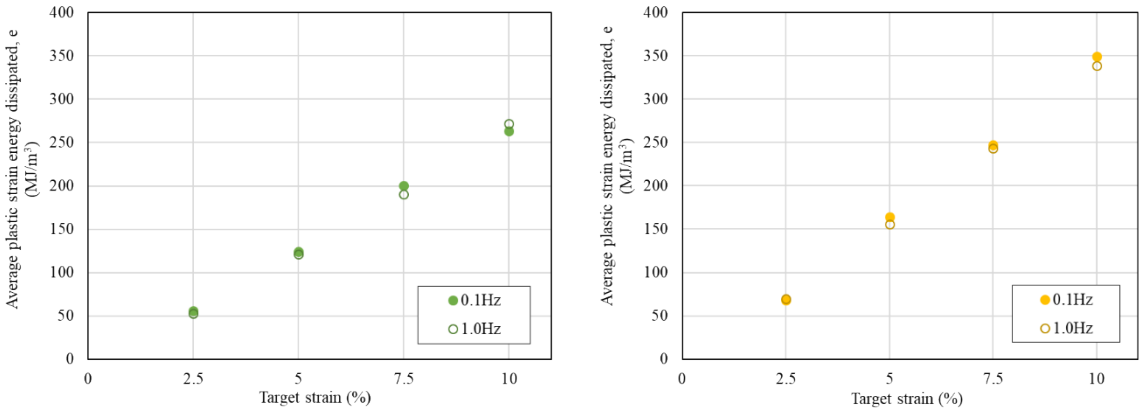

b) Average energy dissipated per unit volume per cycle

Figure 16 Energy dissipated per unit volume of both S355 and S690 steels under Loading Protocol C

Table 1 Chemical compositions of S355 and S690 steels to EN 10025

Steel Grade		C	Si	Mn	P	S	N	B	Cr	Cu	Mo	Nb	Ni	Ti	V	Jr
S355	BS EN 10025-2	0.23	0.6	1.7	0.035	0.035	0.014	-	-	0.6	-	-	-	-	-	-
S690	BS EN 10025-6	0.22	0.86	1.8	0.025	0.012	0.016	0.006	1.6	0.55	0.74	0.07	2.1	0.07	0.14	0.17

Table 2 Monotonic tensile tests of S355 and S690 steels

a) Test programme

Coupon	Shape of coupons	Thickness of steel plates (mm)	Diameter d (mm)	Gauge length L_0 (mm)	Total length L (mm)
S355-T1 S355-T2	Funnel-shaped	10	5	10	184
S690-T1 S690-T2	Funnel-shaped	10	5	10	184

b) Mechanical properties

Coupon	Thickness of original plates (mm)	Young's modulus E (kN/mm^2)	Yield strength f_y (N/mm^2)	Tensile strength f_u (N/mm^2)	Elongation at fracture ε_L (%)	f_u/f_y
S355-T1	10	213.5	387	591	24.4	1.53
S355-T2		221.2	419	619	22.7	1.48
	Average	217.3	403	605	23.6	1.50
	COV	0.018	0.040	0.032	0.036	0.017
S690-T1	10	231.3	872	922	24.1	1.06
S690-T2		225.8	895	933	23.6	1.04
	Average	228.6	883	927	23.8	1.05
	COV	0.012	0.013	0.006	0.011	0.007

Table 3 Test programme of cyclic tests of S355 and S690 steels

a) Funnel-shaped coupons of S355 steels

Thickness of steel plates (mm)	Diameter d (mm)	Gauge length L_0 (mm)	Loading protocol	Loading frequency f (Hz)	Target strain amplitude, ε_m			
					±2.5%	±5.0%	±7.5%	±10.0%
10	5	10	C	0.1	1	1	1	1
				1.0	1	1	1	1
			V	0.1	1	1	1	1
				1.0	1	1	1	1

b) Funnel-shaped coupons of S690 steels

Thickness of steel plates (mm)	Diameter d (mm)	Gauge length L_0 (mm)	Loading protocol	Loading frequency f (Hz)	Target strain amplitude, ε_m			
					±2.5%	±5.0%	±7.5%	±10.0%
10	5	10	C	0.1	1	1	1	1
				1.0	1	1	1	1
			V	0.1	1	1	1	1
				1.0	1	1	1	1

Table 4. Test results of cyclic tests of S355 and S690 steels.

a) Coupons of S355 steels

Thickness of steel plates (mm)	Diameter d (mm)	Gauge length L_0 (mm)	Loading Protocol	Loading frequency f (Hz)	No. of cycles completed, n_c			
					±2.5%	±5.0%	±7.5%	±10.0%
10	5	10	C	0.1	85	13	5	4
				1.0	89	14	7	3
			V	0.1	20	20	20	19
				1.0	20	20	20	19

b) Coupons of S690 steels

Thickness of steel plates (mm)	Diameter d (mm)	Gauge length L_0 (mm)	Loading Protocol	Loading frequency f (Hz)	No. of cycles completed, n_c			
					±2.5%	±5.0%	±7.5%	±10.0%
10	5	10	C	0.1	58	16	8	6
				1.0	54	17	9	5
			V	0.1	20	20	20	19
				1.0	20	20	20	19

Table 5 Energy dissipated per unit volume of steel in cyclic tests of S355 and S690 steels

a) Total energy dissipated per unit volume, E

Loading Protocol C	Target strain ε_m (%)	Total energy dissipated per unit volume E (MJ/m^3)		E_1 / E_o
		E_o S355 steels	E_1 S690 steels	
Loading frequency, f = 0.1 Hz	±2.5	4,732	3,966	0.84
	±5.0	1,615	2,628	1.63
	±7.5	1,001	1,977	1.98
	±10.0	1,054	2,096	1.99
Loading frequency, f = 1.0 Hz	±2.5	4,681	3,772	0.81
	±5.0	1,695	2,651	1.56
	±7.5	1,333	2,188	1.64
	±10.0	816	1,694	2.07

b) Average energy dissipated per unit volume per cycle, e

Loading Protocol C	Target strain ε_m (%)	Average energy dissipated per unit volume per cycle e (MJ/m^3)		e_1 / e_o
		e_o S355 steels	e_1 S690 steels	
Loading frequency, f = 0.1 Hz	±2.5	55.7	68.4	1.23
	±5.0	124.2	164.3	1.32
	±7.5	200.1	247.1	1.23
	±10.0	263.4	349.3	1.33
Loading frequency, f = 1.0 Hz	±2.5	52.6	69.9	1.33
	±5.0	121.1	155.9	1.29
	±7.5	190.4	243.1	1.28
	±10.0	272.1	338.7	1.24

Note: Refer to the measured engineering stress-strain curves shown in Figures 7 to 11.